九州大学学術情報リポジトリ
Kyushu University Institutional Repository

Development of a Passive Reactor Shutdown Device to Prevent Core Disruptive Accidents in Fast Reactors: A Study on Device Specifications

Morita, Koji
Department of Applied Quantum Physics and Nuclear Engineering, Faculty of Engineering, Kyushu University

Liu, Wei
Department of Applied Quantum Physics and Nuclear Engineering, Faculty of Engineering, Kyushu University

Arima, Tatsumi
Department of Applied Quantum Physics and Nuclear Engineering, Faculty of Engineering, Kyushu University

Arita, Yuji
Research Institute of Nuclear Engineering, University of Fukui

他

https://hdl.handle.net/2324/7174404

出版情報：Journal of Nuclear Engineering and Radiation Science. 9 (4), pp.041102-, 2023-03-14. ASME International
バージョン：
権利関係：

KYUSHU UNIVERSITY

Development of a Passive Reactor Shutdown Device to Prevent Core Disruptive Accidents in Fast Reactors: A Study on Device Specifications

Koji Morita[1]
Kyushu University
744 Motooka, Nishi-ku, Fukuoka 819-0395, Japan
morita@nucl.kyushu-u.ac.jp

Wei Liu
Kyushu University
744 Motooka, Nishi-ku, Fukuoka 819-0395, Japan
liuwei@nucl.kyushu-u.ac.jp

Tatsumi Arima
Kyushu University
744 Motooka, Nishi-ku, Fukuoka 819-0395, Japan
arima@nucl.kyushu-u.ac.jp

Yuji Arita
University of Fukui
1-3-33 Kanawa-cho, Tsuruga-shi, Fukui 914-0055, Japan
arita@u-fukui.ac.jp

Isamu Sato
Tokyo City University
1-28-1 Tamazutsumi, Setagaya-ku, Tokyo, 158-8557, Japan
isato@tcu.ac.jp

Haruaki Matsuura
Tokyo City University
1-28-1 Tamazutsumi, Setagaya-ku, Tokyo, 158-8557, Japan
hmatuura@tcu.ac.jp

Yoshihiro Sekio
Japan Atomic Energy Agency
4002 Narita-cho, Oarai-machi, Higashi-ibaraki-gun, Ibaraki 311-1393, Japan

[1] Corresponding author.

sekio.yoshihiro@jaea.go.jp

Hiroshi Sagara
Tokyo Institute of Technology
2-12-1 Ookayama, Meguro-ku, Tokyo 152-8550, Japan
sagara@lane.iir.titech.ac.jp

Masatoshi Kawashima
Tokyo Institute of Technology
2-12-1 Ookayama, Meguro-ku, Tokyo 152-8550, Japan
m.kawashima@lane.iir.titech.ac.jp

ABSTRACT

A new subassembly-type passive reactor shutdown device is proposed to expand the diversity and robustness of core disruptive accident prevention measures for Sodium-cooled Fast Reactors (SFRs). The device contains pins with a fuel material that is in a solid state during normal operation but melts and fluidizes during an Unprotected Loss Of Flow (ULOF) or Unprotected Transient OverPower (UTOP) accident. By rapidly transferring the liquefied device fuel into the lower plenum region of the pins via gravitation alone, the device passively provides high negative reactivity to the core. This study evaluated the nuclear and thermal properties of the device subassembly with metallic fuel to determine the device specifications for proper device operation during a ULOF and UTOP accidents. The results of the transient analysis of the ULOF initiating phase in a 750-MW_{el}-class mixed-oxide-fueled SFR core confirmed that a conventional homogeneous core maintains stable cooling of the core prior to coolant boiling in the driver fuel subassemblies. In contrast, the negative reactivity required to terminate the event by device operation was slightly higher in the low sodium void reactivity core than in the conventional homogeneous core.

1 INTRODUCTION

Since the accident at the Fukushima Nuclear Power Plant (NPP), it has become increasingly important to consider measures to prevent and mitigate the consequences of severe accidents in Design Extension Conditions (DECs), including severe accidents that exceed the design basis accidents in the defense-in-depth concept. In addition to active reactor shutdown systems, the Self-Actuated Shutdown System (SASS) [1] and Gas Expansion Module (GEM) [2] have been developed as passive safety equipment against an Anticipated Transient Without Scram (ATWS) to prevent Core Disruptive Accidents (CDAs) in fast reactors [3, 4]. Furthermore, design measures to establish In-Vessel Retention (IVR) that mitigates the effects of severe accidents and prevents large-scale mechanical energy release during CDA (i.e., energetics) have been proposed as a practical approach to ensure the containment function of radioactive materials [5, 6, 7].

This study aims to significantly improve the safety of Sodium-cooled Fast Reactors (SFRs) by developing a new subassembly-type passive reactor shutdown device that provides “versatility” and “robustness” in preventing the occurrence of CDA in a four-year plan starting in Japanese fiscal year 2019. This device, which replaces some of normal fuel subassemblies and is loaded as a passive shutdown mechanism in the fourth layer of the defense-in-depth concept, maintains the subcritical state and prevents core damage by moving (relocating) the liquefied fuel in device pins to a region with low reactivity worth by simple physical phenomena in the event of an accident.

Kyushu University, University of Fukui, Tokyo City University, Japan Atomic Energy Agency, and Tokyo Institute of Technology participated in this study. This study

aims to demonstrate the engineering feasibility and viability of the device by comprehensively examining the candidate fuel materials used in the device, the pin structure to achieve fuel relocation during an accident, and the nuclear- and thermal-hydraulic characteristics during device operation.

A previous study [8] performed a preliminary evaluation of the device response and the characteristics of the device-loaded core for the candidate device specifications to understand the transient dynamic characteristics of the core during device operation. The device operating conditions were outlined for stable core cooling before coolant boiling in driver fuel subassemblies and termination of both initiating events during an Unprotected Loss Of Flow (ULOF) and an Unprotected Transient OverPower (UTOP) accident in a Mixed-OXide (MOX) fueled SFR core loaded with the device. Based on the preliminary results of that study, we determined the device structure and device specifications to maximize the device's effectiveness and studied the installation method of the device in the core. Furthermore, transient characteristics during a ULOF and UTOP of device-loaded cores were evaluated for a conventional homogeneous core and a low sodium void reactivity core.

2 DEVICE STRUCTURE DESIGN CONCEPT

The device proposed in this study is a subassembly of bundled pins containing low-melting-point fuel that is solid under core temperature conditions during normal operation and liquefies because of a rise in its temperature during an accident. The device is immediately activated by the gravity-induced movement of the liquid-phase

fuel in the device pins during an accident, and a high negative reactivity is imposed by the movement of the liquid-phase fuel into the lower plenum region.

In satisfying this operating principle, the reference device specification proposed in the previous study uses a U-Pu-Fe alloy as the device fuel, which has the characteristics of fast reactor fuel and a relatively low melting point. Given swelling caused by fuel burnup, the device structure is designed with hollow fuel pellets, which facilitates the movement of liquefied fuel during device operation (Figure 1). During device operation, liquefied fuel flows down along the hollow wall of device fuel pellets [8].

As liquid-phase fuel moves within the device fuel pin, it may resolidify on the hollow wall of the device fuel pellet, inhibiting the continued flow of liquefied fuel within the pin and plugging the flow path. Therefore, a preheating pin with the same diameter as the device fuel pin is installed separately from the device fuel pin to prevent the solidification of liquid-phase fuel by raising the coolant temperature flowing through the device subassemblies to a predetermined level during normal operation [8]. In this study, the preheating pin fuel was placed below the lower end of the lower blanket region of the driver fuel from the viewpoint of preventing recriticality when the device fuel is relocated because of device operation.

Furthermore, the preheating fuel was placed in the device fuel pin at the same height as the lower component of the device fuel and the fuel-loaded position of the preheating pin to increase the preheating capability. The top of the preheating fuel of the device fuel pin is shielded, if necessary, to mitigate the thermal and mechanical

effects from the liquefied fuel that has moved to the lower plenum during device operation. Figure 2 illustrates the axial arrangement concept within the device fuel pin and preheating pin compared with the driver fuel pin.

If extrusion occurs when the burned device fuel melts, the fluidity of the liquefied fuel may deteriorate significantly. Therefore, the lower plenum and device fuel region are separated by a fusible plug (Figure 1). The latter is pre-pressurized to facilitate the movement of liquefied fuel by melting the fusible plug in the event of an accident, which will be considered as an option in the future.

This device subassembly, which has the same shape and dimensions as a conventional fuel subassembly, can be introduced by replacing some of the fuel subassemblies in the core. Furthermore, it has high compatibility with existing core designs because it has the same nuclear characteristics as other solid fuels during normal operation. After device operation, the device fuel that has moved within the device pin remains in the device pin, making it easy to restart the reactor by replacing the device subassemblies [8].

The specifications for the conceptual design of the device structure described above are given in the design of a device-loaded core for a 750 MW_{el}-class MOX-fueled SFR core [9, 10] described in the next chapter.

3 DEVICE-LOADED CORE DESIGN

3.1 Core characteristics for evaluation

As in the previous study [8], nuclear characteristics were calculated using the conventional homogeneous models with a 70-group cross-section set for fast reactors

[11, 12] in combination with an effective cross-section processing code [13]. Power distributions in the core were calculated using a three-dimensional model, and the spatial distributions of the reactivity coefficients were computed for the two-dimensional RZ-model using a diffusion theory code [14]. The characteristics of the core for this study are summarized in Table 1. Two variations from the compact core design of the 750 MW_{el}-class MOX-fueled core [8] were implemented as fast-spectrum cores to increase tolerance against ATWS events. One causes a 20% reduction in the linear power of the MOX fuel in addition to the conventional core-blanket arrangement. The other has a smaller sodium density coefficient in the framework of the "sodium plenum core concept."

Table 2 presents the typical core features and some of the static core characteristics of the two cores and the referenced compact core [8]:

(1) The conventional homogeneous core with a core length of 100 cm, with an upper blanket and a cycle length of 832 days, has a significant positive whole core sodium void reactivity of approximately +$8.0 in a high burnup core with an average burnup of 150,000 MWd/t.

(2) The upper sodium plenum core with an 80-cm core length, a low void reactivity without an upper axial blanket, with sodium plenum, and a cycle length of 333 days is classified as a "low sodium void reactivity core with upper sodium region." For a standard burnup core with an average burnup of approximately 75,000 MWd/t, the sodium void reactivity has a small positive value of $2.9.

As presented in Table 2, the Doppler coefficients for the whole core are similar for the compact core and these two cores. However, the void reactivity is significantly smaller when the sodium plenum region is implemented.

For these two types of core systems, the power distribution, flow rate distribution, and various reactivity coefficient distributions were calculated, and data for transient analysis were prepared.

3.2 Conceptual design of device subassembly

a) Main features of device subassembly

The device fuel material and arrangement in the pins were determined to meet the requirements for the device subassembly under the rated power operation. Specifications for the device subassembly, including pin size, were discussed. The device subassembly consists of two pin types: a device fuel pin with fuel that changes from solid phase to liquid phase under ATWS conditions and moves down the core region, and a preheating pin that functions to heat the coolant to the planned temperature. The outer diameters of these pins are the same to ensure uniform coolant flow in the device subassembly. An alloy of U-Pu-10 mol% Fe was chosen as the device fuel material because of its melting point.

This subassembly-type device features a device fuel pin diameter equivalent to that of the driver fuel pin and an adjustable ratio of device fuel pins to preheating pins. The coolant flow channel area in the device subassembly is also equivalent to that of the driver fuel subassembly, allowing the coolant outlet temperature to be equivalent to

that of the driver fuel subassembly and satisfying the maximum fuel linear power and temperature range requirements during rated operation.

For the alloy fuel, a hollow type was selected; the inner diameter of the hollow was set large enough to enable the fuel melted by an ATWS event to fall easily along the inner surface of the hollow fuel. At the time of the initial new fuel device, the material is set to 25% SD (smear density). The alloy fuel swells with irradiation, and the fuel cross-section expands by up to approximately 30% at a burnup of 2%. Even in this situation, the central void area of the hollow fuel is reduced to approximately 68% of the pin's inner cross-section, and the molten fuel is expected to pass through to the lower pin region.

Because the device fuel must be kept in a solid phase during rated operation and the coolant temperature must be increased to melt the device fuel even at the bottom of the device fuel during ATWS, it is essential to set sufficient coolant heating capacity in the heater section of the device subassembly. For the heater section, an alloy fuel U-Pu-10 wt% Zr was selected, which has a sufficiently higher melting point than the device fuel material, to achieve efficient performance in the limited lower space of the device pin. The device fuel pin heater is set at the bottom of the device fuel pin with a smear density of 75% and low coolant temperature. The fuel in the preheating pin is similarly located at the bottom of the pin. Neutron absorbers were installed on these preheating pins adjacent to the axial region where the molten fuel moves to maintain the reactivity of the whole core sufficiently low after device startup.

In this study, an optimum combination of axial position, axial length, smear density, and fissile fraction (Pu enrichment) of the device fuel was selected so that the reactor reactivity increase can be avoided in the process of device fuel relocation. It was confirmed by static neutronic calculations that the total amount of the device fuel does not lead to recriticality even if it is concentrated in the core region within the device fuel pins.

b) Temperature conditions for device fuel

In this study, a Hot Spot Factor (HSF) and an overpower factor, which is a ratio of the design trip value to the rated power, were applied to the solidus temperature of the device fuel material to set an upper limit for the rated temperature of the device fuel to ensure that the device fuel is solid in rated operating conditions. The assumed HSF was 1.2, and the overpower factor was 1.16, are the design values for the Japanese prototype fast breeder reactor Monju [15]. Assuming a reactor power level error of 2%, the relative uncertainty of the device fuel temperature rise is 1.37 (= 1.2×[1.16–0.02]) because it is superimposed on the overpower condition and fuel temperature uncertainty.

Given the HSF and the overpower factor, the limit temperature (T_{LIM}) to maintain the device fuel solid in rated operation was set at 567°C instead of the solidus temperature of 630°C for the ternary alloy 65.6U-24.4Pu-10Fe (mol%), which is the device fuel material. The coolant flow rate is higher than in rated operation. Above the solidus temperature of the device fuel material, the molten fuel becomes a mixture of liquid and solid phases. The viscosity of the solid-liquid mixture decreases as the fraction

of the solid phase decreases. When the viscosity of the device fuel in the liquid-solid mixture reaches a specific threshold temperature (T_{VIS}), the molten fuel in the device pin can move downward. In this study, a temperature of 695°C, at which the solid phase fraction of the molten device fuel reaches 40%, was selected as one at which the device fuel starts its movement. Above that temperature, the device fuel was assumed to be able to move within the device pin. For this candidate ternary alloy, the temperature gap between T_{VIS} and T_{LIM} is 128°C under the selected design margins (along with the HSF and the overpower factor).

An additional search indicated that a binary alloy of U-10 wt% Fe, Low-Enriched Uranium (LEU), could be the candidate material because the temperature gap between T_{VIS} and T_{LIM} is smaller at 89°C (Table 3). The smaller temperature gap between T_{VIS} and T_{LIM} enforces an earlier start to fuel movement in timelines along the ULOF sequences.

c) Selection of device specifications

Calculations were performed to obtain device characteristics for the cores loaded with 16 device subassemblies. The device subassemblies are scattered in the inner core region where power flattening is achieved. Figure 3 illustrates the core layout of the device subassemblies. This arrangement is commonly applied to device characteristic calculations in the conventional homogeneous core and low sodium void reactivity cores. The flow distribution to the driver fuel subassemblies and the required flow rate were set for each core to satisfy plant performance.

In Figure 4, the device fuel component with U-Pu-Fe alloy and the lower heater element with U-Pu-Zr alloy are indicated by symbols (L), (A), and (C) corresponding to the axial pin locations. For the present survey calculations, the number of device fuel pins per device assembly is assumed to be 240, and the number of preheating pins is assumed to be 91. For the conventional homogeneous core with a height of 100 cm, the 25% Smear Density (SD) hollow device fuel length is set to 30 cm.

The preheating fuels (C) and (A) were assumed to be 20 cm long hollow slags with 25% SD, and (L) was assumed to be 40 cm long with 75% SD. For the low sodium void-worth core with a height of 80 cm, the length of hollow device fuel with 25% SD was set to 40 cm because a more extensive inventory of device fuels is desirable to compensate for the high plutonium (Pu) enrichment core. The preheating fuels (A) and (L) were 20 cm long hollow slag with 25% SD and 40 cm long hollow slag with 75% SD. The preheating fuel section (C) was removed.

Preliminary static evaluations assuming a certain power-to-flow ratio suggest that the heating ratio and temperature of the lower end of preheating fuel (A) are critical for preventing the molten device fuel from resolidifying in the core region and maintaining molten fuel fluidity during a ULOF.

The nuclear characteristic survey calculations were performed using the ratio of Pu to uranium (U) in the device fuel and preheating fuel materials as parameters, with Pu:U of 1:1, 1:2, and 1:3. The method of survey calculations is briefly described in our previous study [8]. The results of these calculations are summarized in Figure 5 as the ranges selected as specifications for the device subassembly. Some combinations of

device fuels with high Pu fractions were not selected because the line heat rating and flow rate requirements were excessive.

We identified the role of the device fuel pins and the lower heater sections in these survey calculations. A combination of a device fuel with a power of approximately 1.5 MW_{th} and a lower heater with a power of approximately 3.5 MW_{th} was an appropriate candidate for selecting device specifications. Within the range obtained, we selected device fuel with a Pu:U of 1:3 and preheating fuel with a Pu:U = 1:1. This combination is estimated to provide a total reactivity worth of –$1.86 for the 16 device subassemblies.

4 SAFETY ANALYSIS OF DEVICE-LOADED CORES

Transient dynamic characteristics during device operation were evaluated for a 750 MW_{el}-class MOX-fueled SFR core to calculate device performance during a ULOF and UTOP. The effect of asynchrony on the device reactivity insertion on the termination of an initiating phase of ULOF was also confirmed.

4.1 Transient core characteristics

Transient behavior analyses were performed for two types of cores whose specifications were determined in the previous chapter—the conventional homogeneous core and the low sodium void reactivity core. Transient behavior significantly impacts ULOF behavior.

Based on the power and reactivity characteristics of the core studied in the previous chapter, the transient characteristics of the target core without device

operation in the “initiating phase” of ULOF and UTOP were analyzed using the transient analysis code ARGO [5] based on the flow network model as a dynamic evaluation model. Initiating conditions for ULOF and UTOP were determined based on the representative conditions in the licensing safety analysis of Monju [15]. For ULOF, the coolant flow half-time through the core was set to 5 s. For UTOP, a control rod with a reactivity value of $0.90 was assumed to be withdrawn in 30 s, which is the maximum control rod withdrawal rate set as a typical TOP condition, and the coolant flow rate was assumed to be the same as the rated value. This relatively long reactivity insertion time was assumed so the fuel temperature increase could be evaluated conservatively.

The evaluation results of ULOF for the conventional core and the low sodium void reactivity core without device operation are depicted in Figure 6. The variations in power *P*, coolant flow rate *F*, and power to coolant-flow ratio (*P*/*F*) over time are depicted as values relative to the start of ULOF. The low sodium void reactivity core has a slower power increase at ULOF than the conventional core with high void reactivity; the power becomes static because negative reactivity is inserted from coolant boiling. However, as the flow rate decreases, *P*/*F* increases again. Because the flow rate decrease causes boiling in the axial core center region where the void reactivity is significant, the *P*/*F* rises to approximately 5 at around 40 s, and a rapid power increase occurs at around 55 s.

Based on these results, it is likely that for the low sodium void reactivity core, the ULOF progresses slower than in the conventional core in the stage of the small void region in the early boiling stage. However, the event is not terminated because of the

expansion of the boiling region. For the UTOP, the peak value of *P*/*F* for the conventional core is approximately 2.0, rising only to 1.7 for the low sodium void reactivity core (Figure 7). For the UTOP, the event is expected to be terminated after this, with a decrease in the reactor power. We discuss ULOF, which is more likely to progress the event, in the next section.

4.2 Device response characteristics in ULOF

The reactivity for all 16 device subassemblies when the device fuel is moved out of the core region is –$1.86. The device fuel has flowability when its temperature exceeds the solidus temperature to some extent before it fully enters the liquid phase. In this study, this initiation temperature of fuel movement was tentatively set to 695°C, the temperature at which the solid phase fraction in the molten fuel is 40%. The device fuel that reaches the initiation temperature of fuel movement is assumed to flow down by gravity along the hollow wall of the fuel pellets, subject to wall friction. In this study, the time required for the molten device fuel to move out of the core region was assumed to be proportional to the axial height of the device fuel from the lower end of the core. The time required for the device fuel to move out of the core region from the upper end of the device fuel region (i.e., the center of the axial height of the core) was set to 0.8 s, obtained by a simplified evaluation.

Figure 8 illustrates the time variation in the *P*/*F* at the ULOF for (a) the conventional homogeneous core and (b) the low sodium void reactivity core. In the conventional homogeneous core, device operation terminates the event without coolant boiling. In the low sodium void reactivity core, the power decreases when 60%

of the fuel (24 cm from the top) flows out of the core. The power continues to decrease, although the device reactivity is not inserted because of the decrease in device fuel temperature. However, the coolant begins to boil around 30 s after the start of the transient.

The coolant temperatures at the top and center of the core of the fuel subassembly with a large *P*/*F* are examined in Figure 9. The coolant temperature reaches a constant temperature at the core top height at around 28 s, indicating that coolant boiling has started. The coolant at the core middle height also starts boiling at around 32 s, at which time a power surge occurs, the device fuel moves, negative reactivity is inserted, and the power decreases. However, because the coolant boiling continues, although the net reactivity in the core is still negative, the fuel temperature should continue rising in a generally adiabatic state, leading to the melting of the fuel pins. Thus, the device operation reduces the reactor power in the low sodium void reactivity core, but the event termination is not expected because of the coolant boiling. Therefore, it is necessary to avoid coolant boiling in the low sodium void reactivity core by enhancing device reactivity.

Additional evaluations in the case of the binary alloy (U-10 w% Fe) device fuel were performed with the same calculation conditions for a ternary alloy device except for temperatures of T_{VIS} and T_{LIM}. Figure 10 illustrates the time variation in the *P*/*F* at ULOF for (a) the conventional homogeneous core and (b) the low sodium void reactivity core. In the case of U-10 wt% Fe device fuel, T_{LIM} at the rated state can be raised by approximately 70°C (from 567°C to 636°C). In contrast, T_{VIS} rises by approximately 30°C

from 695°C to 725°C. The device responds faster compared with the cases with the ternary alloy device fuel.

In the conventional case, a smaller *P*/*F* level at around 20 s is attained, and the same *P*/*F* levels occur at around 50 s, compared with the *P*/*F* curve in Figure 8(a). After 50 s, power and *P*/*F* continue to decrease. In the low sodium void reactivity core, *P*/*F* continues to decrease after 50 s without the coolant boiling, contrary to the case depicted in Figure 8(b)—the timing of inserting the device reactivity is earlier because of the smaller temperature gaps between T_{VIS} and T_{LIM} of the binary alloy U-10 wt% Fe. The negative reactivity necessary for terminating the event is inserted before boiling.

4.3 Evaluation of the effect of asynchronous device operation

Asynchronies in device operation because of axial temperature differences within the device pins were considered in the previous section. However, the power differences depending on the in-core location of the device subassemblies and temporal power variations, differences in coolant flow rates among the subassemblies, coolant flow distribution within the subassembly, power distribution (peaking) within the subassembly, and device fuel properties affected by burnup (thermal conduction changes) may also cause differences in device operating time.

Of these, the radial power distribution in the core and peaking in the subassembly contribute significantly to the asynchronous behavior of the device. Therefore, the effects on device operation asynchrony are represented here by high- and low-power device subassemblies. Those conditions are presented in Table 4. We further assumed that the high- and low-power device subassemblies represent half of

the total device subassemblies. The overall device reactivity was set to –$1.86. In the following transient analysis considering asynchronous device operation, the ULOF in the conventional homogeneous core is considered.

Figure 11 (a) illustrates the time variation in *P*, *F* and *P*/*F* during a ULOF under the above conditions and considering asynchronous device operation. For a high-power device subassembly with a relative power of 1.2 times, device reactivity is inserted by starting the operation early in the transient (around 5 s). However, the reduction in reactor power resulting from device operation is minimal compared with the case where devices operate simultaneously. The low-power subassembly with 0.8 times relative power starts operating at high *P*/*F* (around 25 s after the transient starts). Nonetheless, the reduction effect of reactor power during device operation is also minimal, so coolant boiling occurs and the event is not terminated. Therefore, if the magnitude of device reactivity in the entire core increases, the event can be terminated by a high negative device reactivity inserted during high-power device subassembly operation. Consequently, the low-power device subassembly operates with a delay.

The total reactivity required to terminate the ULOF event with only the high-power device subassembly was examined with these considerations. As depicted in Figure 11 (b), when the magnitude of device reactivity for the entire core is multiplied by 1.3 (1.3 × –$1.86 = –$2.40), the event is terminated with the reactivity of the low-power device subassembly, which operates with a delay. However, the event is not terminated at 1.2 times because of coolant boiling at the end. The total reactivity required to stop the ULOF event is approximately –$2.40, indicating the necessity of

increasing the number of device subassemblies or the device reactivity by increasing the enrichment of the device fuel.

5 CONCLUDING REMARKS

The specifications of a new subassembly-type passive reactor shutdown device that increases the versatility and robustness of measures to prevent CDAs in SFRs are discussed. Two types of candidate materials for the device fuels are selected: (1) U-Pu-Fe ternary alloy and (2) LEU-Fe binary alloy. The device structure and in-core installation method to maximize device effectiveness in 750 MW_{el}-class MOX-fueled SFR cores were investigated, and the transient dynamic characteristics during device operation were evaluated. We clarified the device's effectiveness for large MOX-fueled SFR cores, regardless of the magnitude of the positive void reactivity.

Compared with the device reactivity that terminates a ULOF event in the conventional homogeneous core, the device reactivity must be increased in the low sodium void reactivity core to avoid a void state in the sodium plenum region because of coolant boiling. The results also indicate that the number of device subassemblies to be loaded may need to increase to terminate ULOF events, even when asynchronous device operation from power distribution among and within device subassemblies is also considered. In the future, we will conduct optimization studies on the ratio of device fuel pins to preheating pins to increase device performance, materials inside the pins, and the number of device subassemblies required and other factors to improve device performance.

ACKNOWLEDGMENT

Special thanks to Dr. Yasushi Tsuboi of Toshiba Energy Systems & Solution Corp. We are deeply grateful to Dr. Hiroshi Endo for collaborating during the early stages of this work. We also thank Philip Pape, Ph.D., from Edanz (https://jp.edanz.com/ac) for editing a draft of this manuscript.

FUNDING

This work was supported by the Ministry of Education, Culture, Sports, Science and Technology (MEXT) Innovative Nuclear Research and Development Program in Japan.

NOMENCLATURE

F	coolant flow rate relative to the start of a transient
P	power relative to the start of a transient
P/F	power to coolant-flow ratio
T_{LIM}	limit temperature to maintain the device fuel solid in rated operation, °C
T_{VIS}	threshold temperature at which the molten fuel in the device pin can move downward, °C

Acronyms and Abbreviations

ATWS	Anticipated Transient Without Scram
ARGO	plant dynamics analysis code
CDA	Core Disruptive Accident
DEC	Design Extension Condition
GEM	Gas Expansion Module
HSF	Hot Spot Factor
IC	Inner Core
IVR	In-Vessel Retention
LEU	Low-Enriched Uranium
MEXT	Ministry of Education, Culture, Sports, Science and Technology
MOX	Mixed OXide

NPP	Nuclear Power Plant
OC	Outer Core
SD	Smear Density
SASS	Self-Actuated Shutdown System
SFR	Sodium-cooled Fast Reactor
ULOF	Unprotected Loss Of Flow
UTOP	Unprotected Transient OverPower

REFERENCES

[1] Sowa, E.S., Barthold, W.P., Eggen, D.T., Huebotter, P.R., Josephson, J., Pizzica, P.A., Turski, R.B., and van Erp, J.B., 1976. LMFBR Self-Actuated Shutdown Systems, Proceedings of the International Meeting on Fast Reactor Safety and Related Physics, Chicago, Illinois, USA, October 5-8, pp. 673-682.

[2] Burke, T.M., 1998. Summary of FY 1997 Work Related to JAPC-US DOE Contract Study on Improvement of Core Safety – Study on GEM (III), HNF-2195-VA. February, 32 pages. Free download from: https://inis.iaea.org/collection/NCLCollectionStore/_Public/30/039/30039909.pdf?r=1&r=1

[3] Tentner, A.M., Parma, E., Wei, T., and Wigeland, R., 2016. Severe Accident Approach – Final Report Evaluation of Design Measures for Severe Accident Prevention and Consequence Mitigation, ANL-GENIV-128, Argonne National Laboratory, Chicago, Illinois, USA, March, 116 pages. Free download from: https://www.osti.gov/biblio/973483

[4] No. NR-T-1.16, 2020. Passive Shutdown Systems for Fast Neutron Reactors, IAEA Nuclear Energy Series, Vienna, Austria, 110 pages. Free download from: https://www.iaea.org/publications/13386/passive-shutdown-systems-for-fast-neutron-reactors

[5] Endo, H., Kumaoka, Y., Golan, S., and Nakagawa, H., 1992. Passive Safety Features of a Bottom Supported Fast Breeder Reactor Vessel, Nuclear Technology, Vol. 99, No. 3, pp. 318-329.

[6] Maschek, W., Flad, M., Boccaccini, C. M., Wang, S., Gabrielli, F., Kriventsev, V., Chen, X., Zhang, D., and Morita, K., 2011. Prevention and Mitigation of Severe Accident Developments and Recriticalities in Advanced Fast Reactor Systems, Progress in Nuclear Energy, Vol. 53, No. 7, pp. 835-841.

[7] Sciora, P., Blanchet, D., Buiron, L., Fontaine, B., Vanier, M., Varaine, F., Venard, C., Massara, S., Scholer, A.C., and Verrier, D.P., 2011. Low Void Effect Core Design Applied on 2400 MWth SFR Reactor, Proceedings of 2011 International Congress on Advances in Nuclear Power Plants (ICAPP 2011), Nice, France, May 2-6, Paper 11048, pp. 487-495. Free download from: https://inis.iaea.org/search/search.aspx?orig_q=RN:44092769

[8] Morita, K., Liu, W., Arima, T., Arita, Y., Kawase, K., Sato, I., Matsuura, H., Sekio, Y., Sagara, H., and Kawashima, M., 2023. Development of a Passive Reactor Shutdown Device to Prevent Core Disruptive Accidents in Fast Reactors: A Preliminary Study, ASME Journal of Nuclear Engineering and Radiation Science, NERS-21-1161 (Research Paper), in press.

[9] JAEA-Research 2006-042, 2006. Feasibility Study on Commercialized Fast Reactor Cycle Systems Technical Study Report of Phase II, - (1) Fast Reactor Plant Systems -, Japan Atomic Energy Agency, Ibaraki, Japan, (in Japanese), 45 pages. Free download from: https://jopss.jaea.go.jp/pdfdata/JAEA-Research-2006-042.pdf

[10] Hayafune, H., Sakamoto, Y., Kotake, S., Aoto, K., Ohshima, J., and Ito, T., 2011. Conceptual Design Study for the Demonstration Reactor of JSFR: (1) Current Status of JSFR Development, Proceedings of the 19th International Conference on Nuclear Engineering (ICONE-19), Chiba, Japan, May 16-19, ICONE19-44140, 9 pages. Free download from: https://www.jstage.jst.go.jp/article/jsmeicone/2011.19/0/2011.19__ICONE1944_46/_article

[11] Sugino, K., Jin, T., Hazam, T., and Numata, K., 2012 Preparation of Fast Reactor Group Constant Sets UFLIB.J40 and JFS-3-J4.0 Based on the JENDL-4.0 Data, JAEA-Data/Code 2011-017, Japan Atomic Energy Agency, Ibaraki, Japan, January, (in Japanese), 52 pages. Free download from: https://jopss.jaea.go.jp/pdfdata/JAEA-Data-Code-2011-017.pdf

[12] Shibata, K., Iwamoto, O., Nakagawa, T., Iwamoto, N., Ichihara, A., Kunieda, S., Chiba, S., Furutaka, K., Otuka, N., Ohsawa, T., Murata, T., Matsunobu, H., Zukeran, A., Kamada, S., and Katakura, J., 2011, JENDL-4.0: A New Library for Nuclear Science and Engineering, Journal of Nuclear Science and Technology, Vol. 48, No. 1, pp. 1-30. Free download from: https://www.tandfonline.com/doi/abs/10.1080/18811248.2011.9711675

[13] Nakagawa, M., and Tsuchihashi, K., 1984. SLAROM: A Code for Cell Homogenization Calculation of Fast Reactor, JAERI 1294, Japan Atomic Energy Research Institute, Ibaraki, Japan, December, 90 pages. Free download from: https://jopss.jaea.go.jp/pdfdata/JAERI-1294.pdf

[14] Derstine, K. L., 1984. DIF3D: A Code to Solve One-, Two-, and Three-Dimensional Finite-Difference Diffusion Theory Problems, ANL-82-64, Argonne National Laboratory, Argonne, Chicago, Illinois, USA, April, 294 pages. Free download from: https://www.osti.gov/biblio/7157044

[15] Power Reactor and Nuclear Fuel Development Corporation, 1980. Application for Reactor Installation Permit: Prototype Fast Breeder Reactor Monju, Tokyo, Japan, December, (in Japanese). National Diet Library Digital Collections, https://dl.ndl.go.jp/pid/9502523

Figure Captions List

Fig. 1 Concept of a passive reactor shutdown device

Fig. 2 Outline of axial arrangement in driver fuel pin, device fuel pin, and preheating pin

Fig. 3 Example of arrangement of 16 device subassemblies in the core (green: device subassembly positions)

Fig. 4 Schematic views of pin arrangement across the device subassembly (right) and vertical material arrangement in each type of pin (left)

Fig. 5 Relationship between the device fuel power sharing and reactivity worth of 16 device subassemblies based on a single device subassembly

Fig. 6 Variation in the power, flow, and *P*/*F* over time for ULOF without device operation

Fig. 7 Variation in the flow and *P*/*F* over time for ULOF without device operation

Fig. 8 Variations in the power, flow, and *P*/*F* over time for ULOF with device operation

Fig. 9 Variation in the coolant temperature over time in a fuel subassembly with a relatively higher *P*/*F* (low sodium void reactivity core)

Fig. 10 Variations in the power, flow, and *P*/*F* over time for ULOF with U-Fe device operation

Fig. 11 Effect of asynchronous device operation on variation in the power, flow, and *P*/*F* over time in conventional homogeneous core

Table Caption List

Table 1 Core specifications for evaluation

Table 2 Reactivity coefficients of the core for evaluation

Table 3 Comparison of limit temperature in rated operation and threshold temperature for flowability of device fuels

Table 4 Device subassembly conditions representative of asynchronous device operation

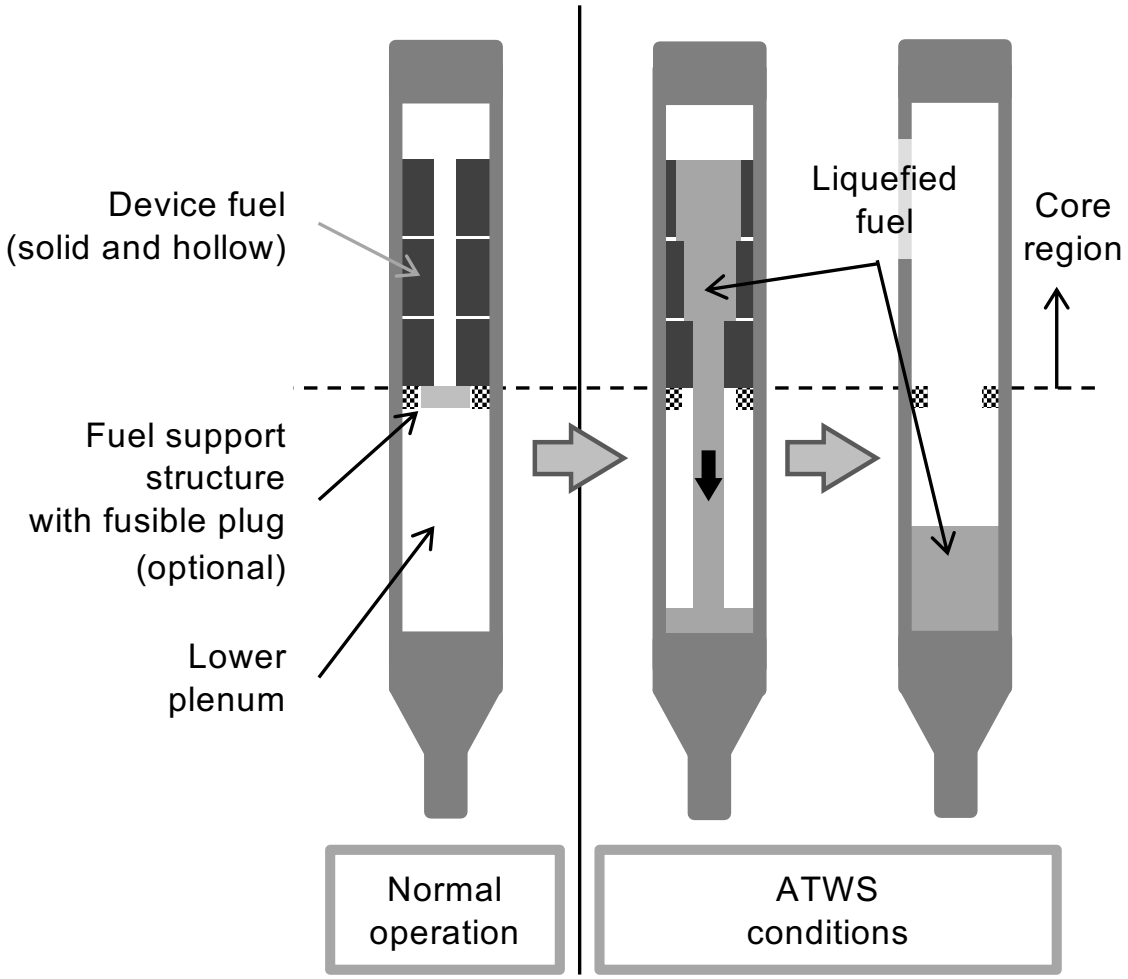

Fig. 1 Concept of a passive reactor shutdown device

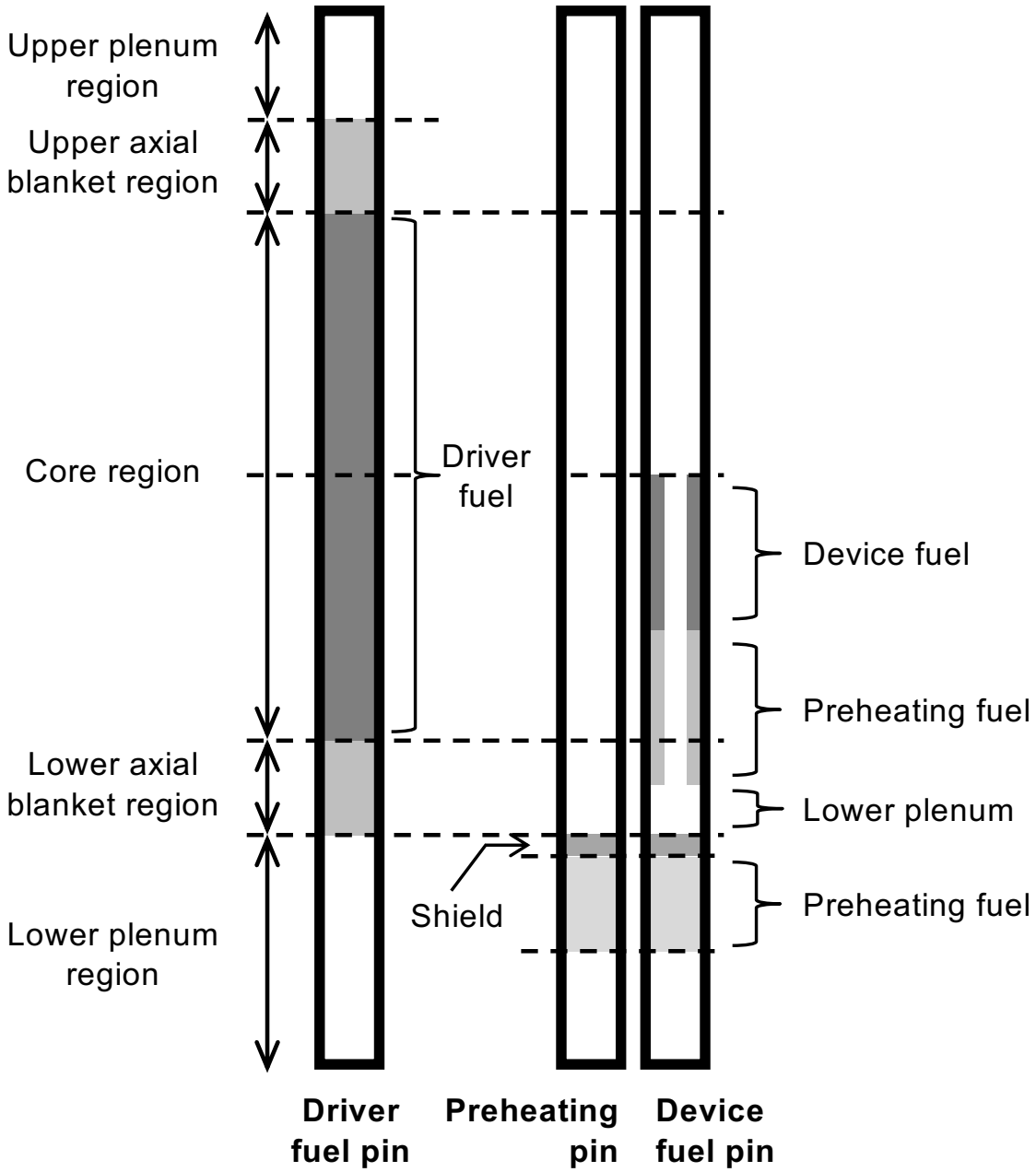

Fig. 2 Outline of axial arrangement in driver fuel pin, device fuel pin, and preheating pin

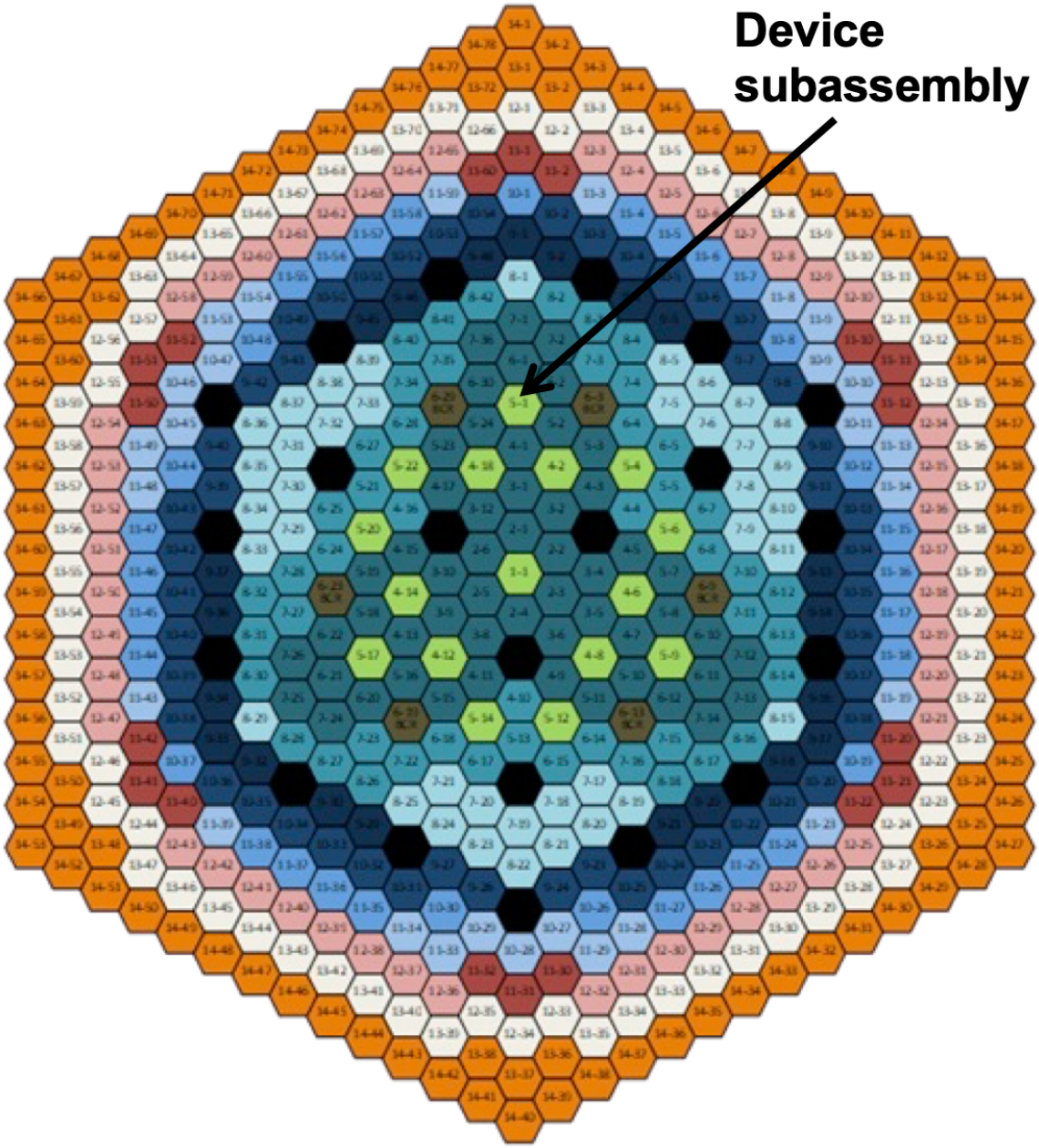

Fig. 3 Example of arrangement of 16 device subassemblies in the core (green: device subassembly positions)

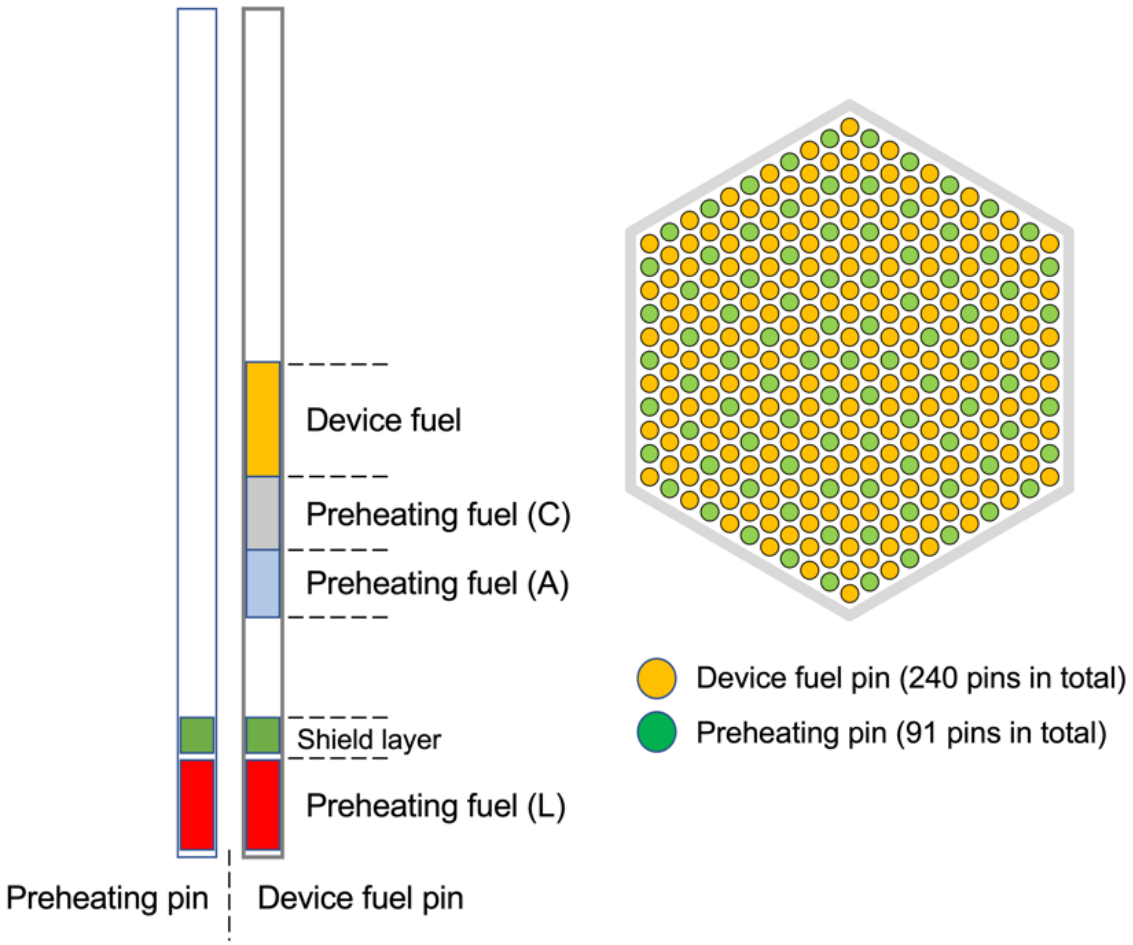

Fig. 4 Schematic views of pin arrangement across the device subassembly (right) and vertical material arrangement in each type of pin (left)

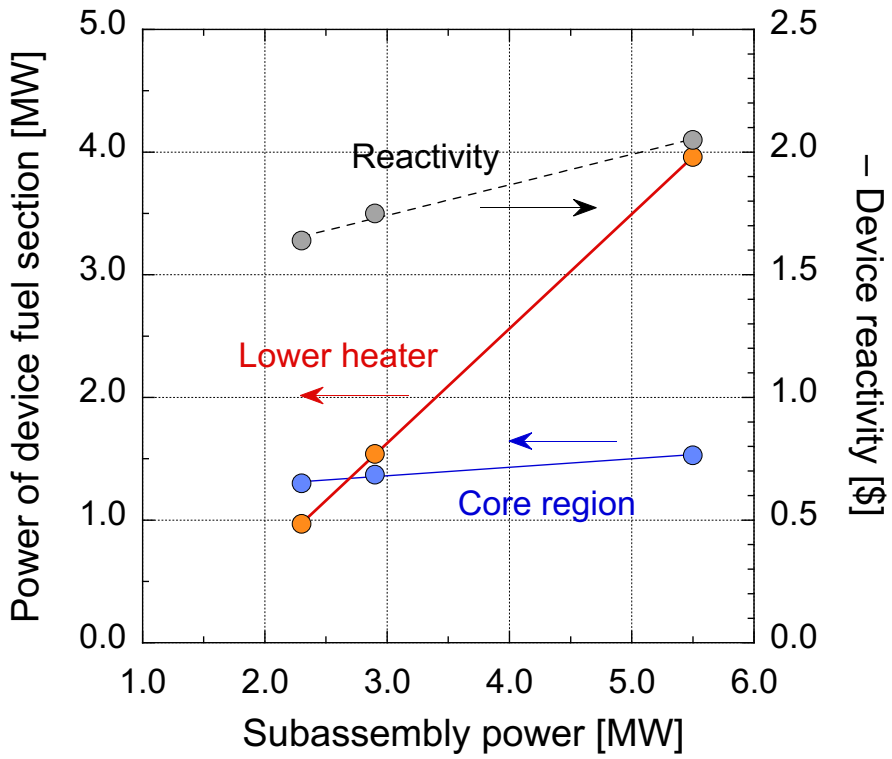

Fig. 5 Relationship between the device fuel power sharing and reactivity worth of 16 device subassemblies based on a single device subassembly

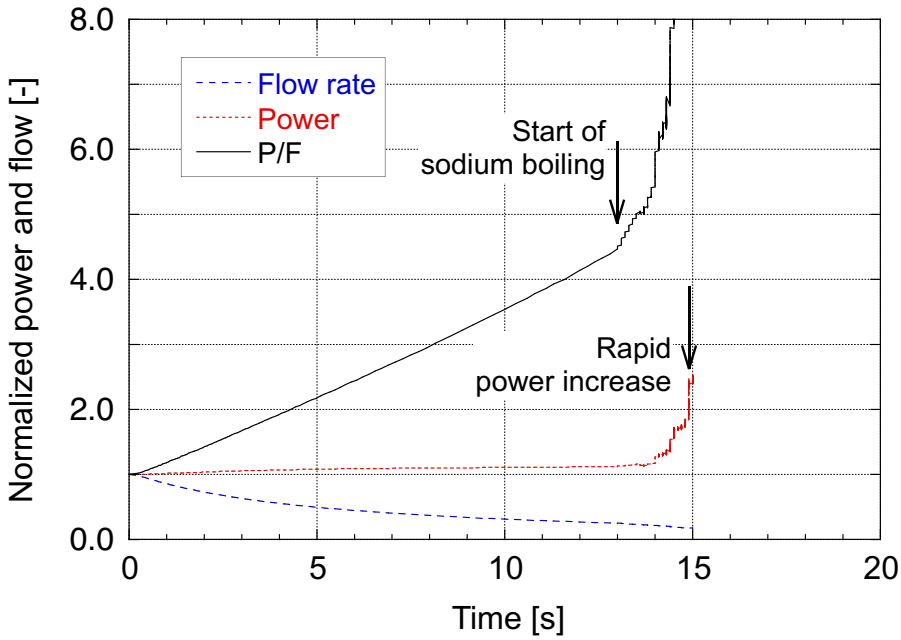

(a) Conventional homogeneous core

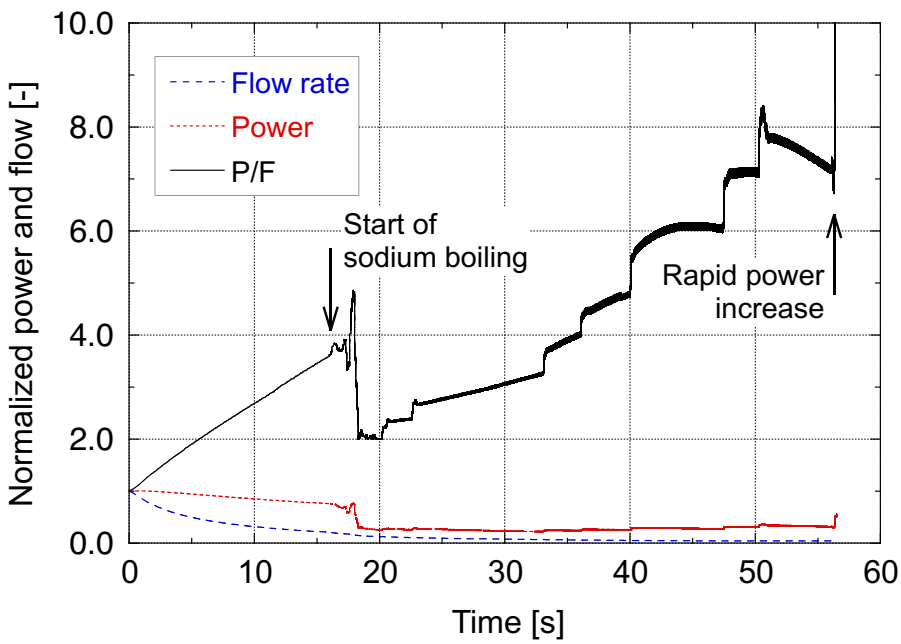

(b) Low sodium void reactivity core

Fig. 6 Variation in the power, flow, and *P*/*F* over time for ULOF without device operation

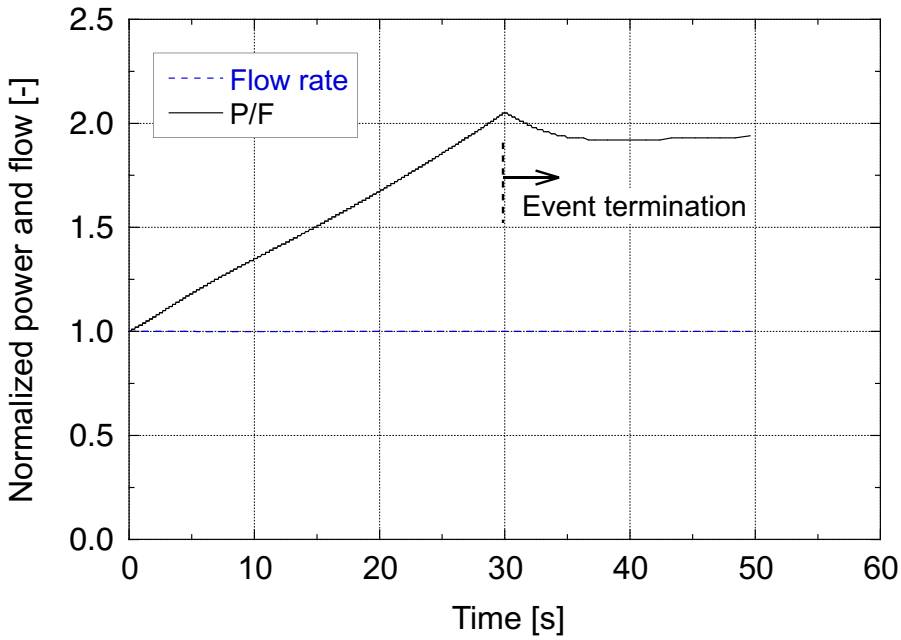

(a) Conventional homogeneous core

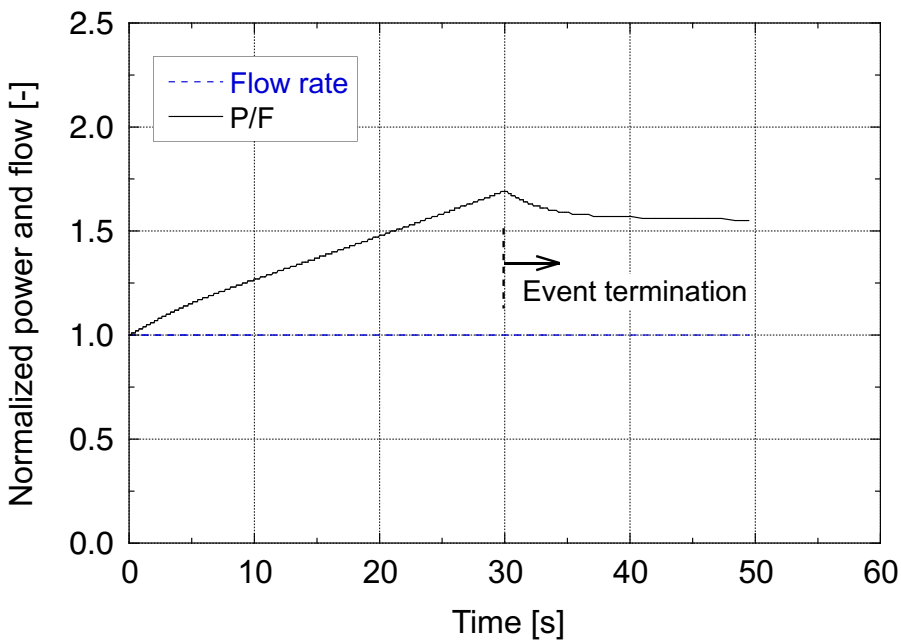

(b) Low sodium void reactivity core

Fig. 7 Variation in the flow and *P*/*F* over time for ULOF without device operation

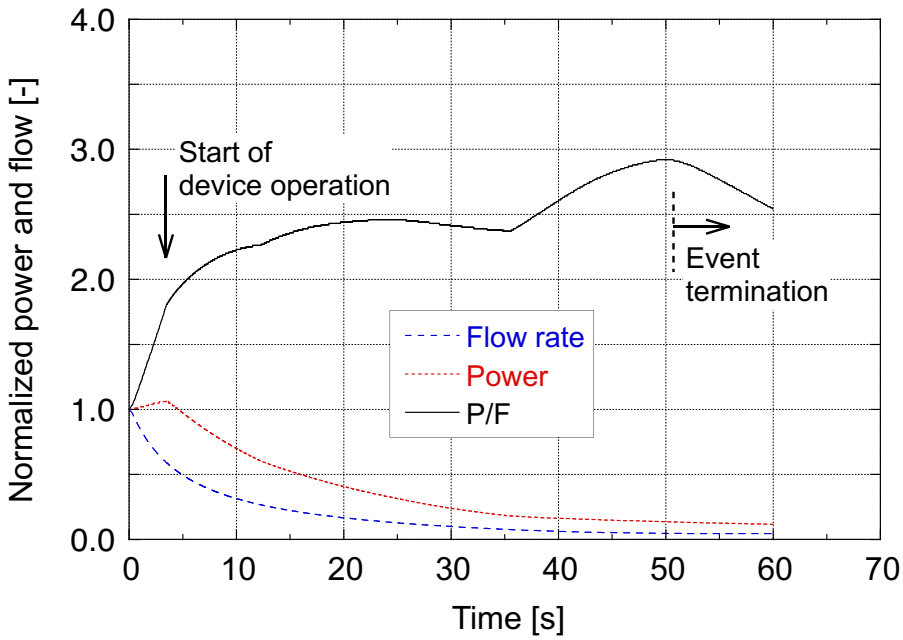

(a) Conventional homogeneous core

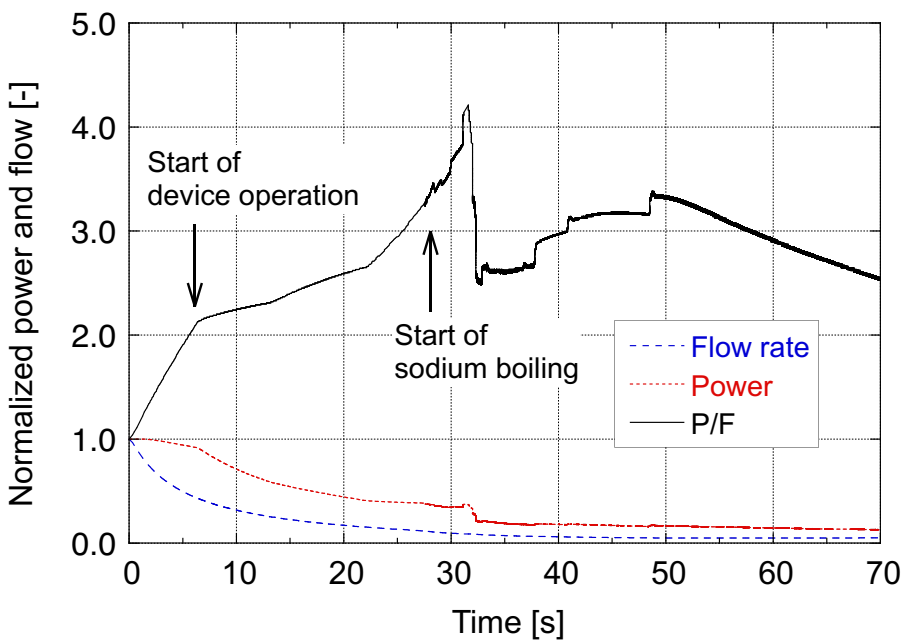

(b) Low sodium void reactivity core

Fig. 8 Variations in the power, flow, and *P*/*F* over time for ULOF with device operation

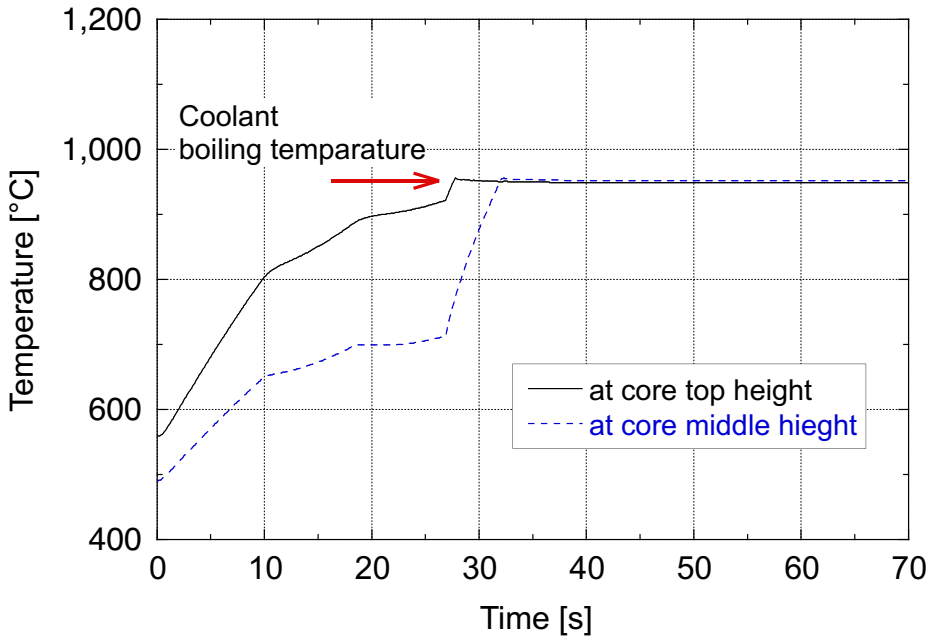

Fig. 9 Variation in the coolant temperature over time in a fuel subassembly with a relatively higher *P*/*F* (low sodium void reactivity core)

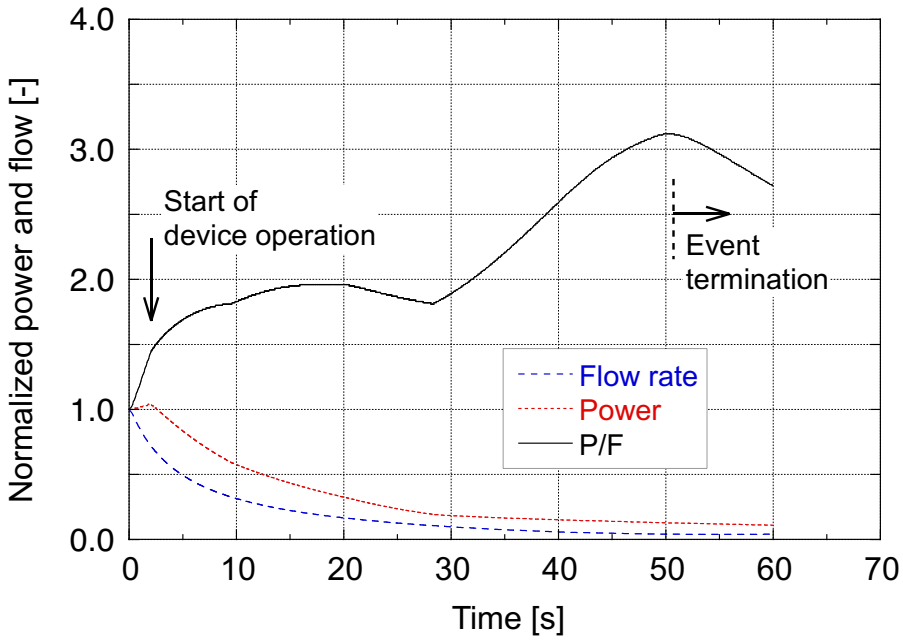

(a) Conventional homogeneous core

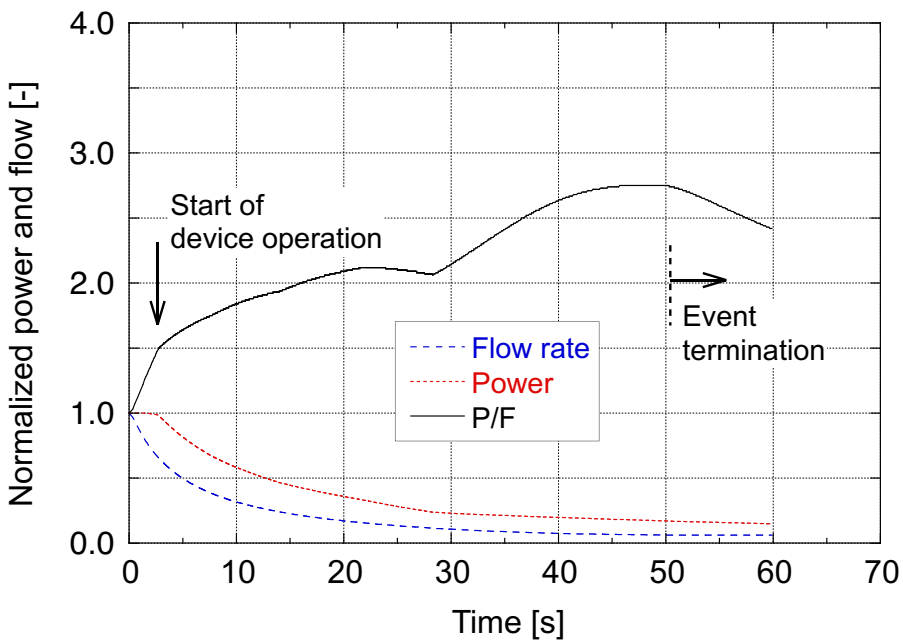

(b) Low sodium void reactivity core

Fig. 10 Variations in the power, flow, and *P*/*F* over time for ULOF with U-Fe device operation

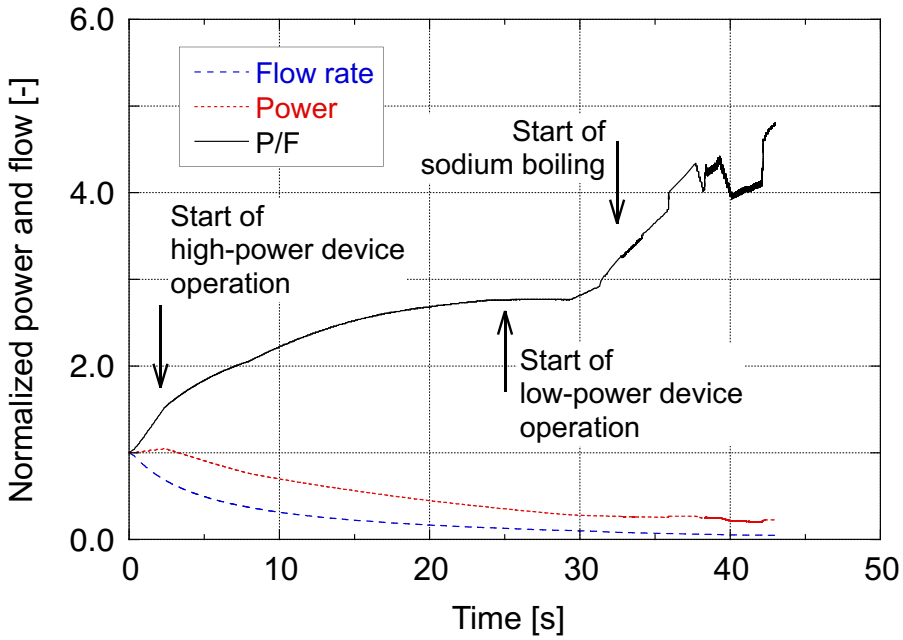

(a) Device reactivity of –$1.86

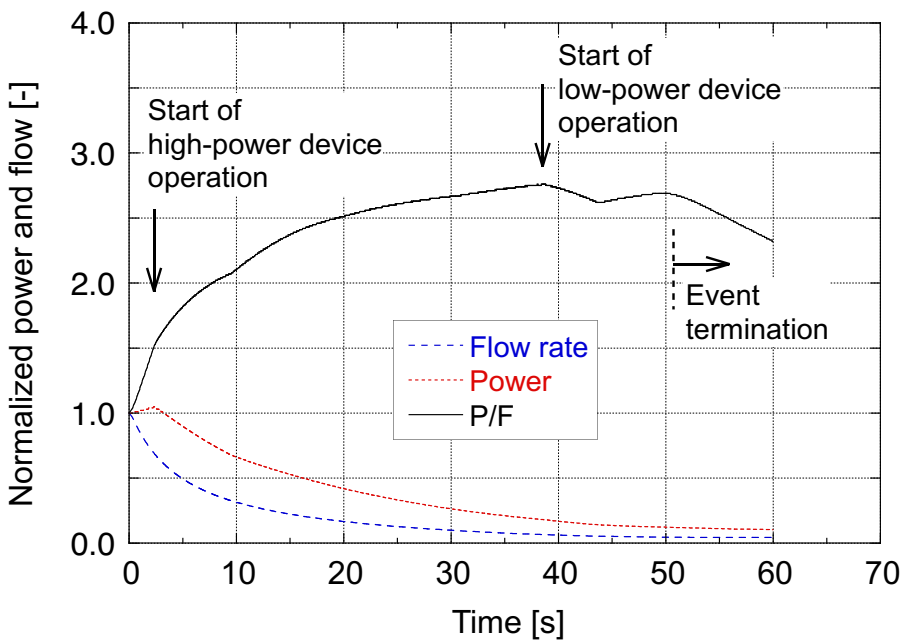

(b) Device reactivity of –$2.40

Fig. 11 Effect of asynchronous device operation on variation in the power, flow, and *P*/*F* over time in conventional homogeneous core

Table 1 Core specifications for evaluation

Reactor power	1785 MW_{th} (750 MW_{el})
Coolant inlet/outlet temperature	395/550ºC
Number of fuel subassemblies	286
Number of blanket subassemblies	66
Primary coolant flow rate	9083 kg/s
Coolant flow rate in fuel subassemblies	8718 kg/s
Number of fuel pins per subassembly	311 *
Pin outer diameter	9.4 mm
Hexagon inside flat-to-flat	191.8 mm
Wrapper thickness	5 mm
Subassembly pitch	206.8 mm

* corresponding to 331 pins for a subassembly without an inner duct

Table 2 Reactivity coefficients of the core for evaluation

	Conventional homogeneous core	Low sodium void reactivity core	Compact homogeneous core [3]
Upper region of core	Blanket	Sodium plenum	Blanket
Core height (cm)	100	80	100
Number of fuel pins per subassembly	311	311	255
Operation cycle length (days)	832	333	832
Average discharge burnup (MWd/kg)	150	75	150
Doppler coefficient (10^{-3} Tdk/dT) IC/OC/(IC+OC)	-4.16 /-1.43 /-5.59	-4.32 /-1.52 /-5.85	-4.09 /-1.41 /-5.50
Sodium void reactivity（$） (IC+OC)/(IC+OC+upper region)	8.1/8.0	5.9/2.9	8.2/8.2

(IC: Inner Core, OC: Outer Core)

Table 3 Comparison of limit temperature in rated operation and threshold temperature for flowability of device fuels

Device fuel	T_{LIM} (°C)	T_{VIS} (°C)	
U-Pu-Fe (Ternary alloy)	567	695	U:Pu:Fe = 65.6:24.4:10 (mol%) solidus temperature: 630°C liquidus temperature: 781°C
U-Fe (Binary alloy)	636	725	U:Fe = 66:34 (mol%) solidus temperature: 725°C liquidus temperature: 725°C

Table 4 Device subassembly conditions representative of asynchronous device operation

	Device subassemblies	
	High power	Low power
Relative power to average	1.2	0.8
Relative coolant flow rate to average	1.1	0.9
Relative device reactivity to average	1.2	0.8
Ratio of number of device fuel subassemblies to total	0.5	0.5